Characterization of the Analog and Digital CMS Pixel Readout Chip after Irradiation

A master thesis submitted to

ETH Zurich

for the degree of

Master of Science in Physics

presented by

Lukas Hoppenau

born on July 2, 1988

citizen of Germany

submitted on July 25, 2013 to

Prof. Dr. Rainer Wallny

Institut of Particle Physics, ETH Zurich

Eidgenössische Technische Hochschule Zürich
Swiss Federal Institute of Technology Zurich

ETH Institute for Particle Physics

Abstract

Within this thesis, irradiation effects on the current analog *PSI46V2* and on the future digital *PSI46digV2* CMS readout chip (ROC) have been investigated. For analog chips, irradiation effects of fluences up to $30 \times 10^{14}\,\mathrm{n}_{eq}/\mathrm{cm}^2$ were analyzed and for digital chips up to $6 \times 10^{14}\,\mathrm{n}_{eq}/\mathrm{cm}^2$. The investigations concentrated on the influence of irradiation effects on the characteristic properties of the *Vtrim* digital to analog converter (DAC) and on the influence of irradiation on different calibration methods. Revealing difficulties to calibrate irradiated ROCs with X-rays due to irradiation defects in the pixel sensor, a new calibration method based on the band gap reference voltage has been successfully implemented. The new method was confirmed by the results of calibrating irradiated ROCs with non-irradiated sensors. Additionally, pulse height DAC optimization has been carried out for the digital *PSI46digV2* chip.

Contents

1 Introduction

In 2009 the Large Hadron Collider (LHC) [7] at CERN[1] started to produce first proton-proton collisions. Now, after almost three years of data taking, the LHC has reached an integrated luminosity of about $25\,\mathrm{fb}^{-1}$ and center-of-mass energies of 8 TeV. The tremendous efforts of the ATLAS and CMS collaborations lead to the discovery of a Higgs boson in 2012 [5, 8].

The search for the Higgs boson and other new physics at the LHC poses a challenge to the experiments. In order to reconstruct the various decay modes of a Higgs boson and to investigate new physics, several subdetectors are used to collect comprehensive information. In this thesis the focus lays on the pixel detector of the CMS experiment which is used to provide both precise primary and secondary vertex reconstruction and track seeding.

Being closest to the beam interaction point, the sensors and readout chips of the pixel detector have to withstand extremely high irradiation fluences. The irradiation intensity on the current pixel detector will further increase after the current shutdown (2013-2014) when the LHC will reach the design luminosity of about $10^{34}\,\mathrm{cm}^{-2}\mathrm{s}^{-1}$ and center-of-mass energies of about 13 TeV. After two additional years of running (2015-2016) with these new conditions, an upgrade of the current pixel detector is planned with one additional pixel layer and a new digital pixel readout chip [19].

Within this thesis, irradiation effects on the current analog *PSI46V2* and on the future digital *PSI46digV2* CMS pixel readout chip (ROC) have been investigated up to an irradiation fluence of $30 \times 10^{14}\,\mathrm{n}_{eq}/\mathrm{cm}^2$ for analog chips and $6 \times 10^{14}\,\mathrm{n}_{eq}/\mathrm{cm}^2$ for digital chips. In particular, irradiation effects on *Vtrim*, one of the Digital to Analog Converters (DAC), were analyzed. The investigations of irradiation defects on this DAC could help to operate the current CMS pixel detector with the analog *PSI46V2* chip in 2015-2016, and could contribute to the development of the future digital *PSI46digV2* chip.

Further, calibration of irradiated chips has been carried out, and the influence of irradiation on different calibration approaches has been studied. This includes the analysis of the calibration of irradiated chips with X-rays, the analysis of the calibration of irradiated chips with a new developed method based on the band gap reference voltage, and the calibration of irradiated ROCs with non-irradiated sensors. The calibration results could serve as an input to Monte-Carlo simulation of the detector response which is a crucial component for physics analysis. Additionally, pulse height DAC optimization was performed for digital chips.

The thesis is organized as follows: In sec. 2 the physics program of the LHC and the CMS experiment are explained, detailing the CMS pixel detector; in sec. 3 irradiation effects on semiconductors and electronic devices are discussed; sec. 4 lays out the experimental methods which are used for investigating the irradiated analog and digital chips; the measurements and results are presented and discussed in sec. 5; finally sec. 6 summarizes the findings and gives possible perspectives on further investigations.

[1] The European Organization for Nuclear Research.

2 The CMS Experiment at the LHC

In this section the CMS detector and its physics goals at the LHC are briefly presented. The CMS pixel barrel detector, which has been investigated within this thesis, is then discussed.

2.1 Physics at the LHC: Search for Electroweak Symmetry Breaking and Beyond

One of the main goals of the LHC was to find evidence for electroweak symmetry breaking and the Higgs mechanism within the Standard Model [11]. The Standard Model describes the fundamental particles and their interactions. On July 4, 2012, the discovery of a Higgs boson at mass of 125 GeV was announced by the CMS and ATLAS collaborations [5, 8]. Further data taking will now provide more and more insights about the properties of this particle and whether it is compatible with the Standard Model Higgs boson.

In addition to the Higgs search, the LHC allows to investigate a wide range of physics: Although being tested to very high precision, the Standard Model is still incomplete and has to be further studied. Questions about phenomena such as Dark Matter or baryon asymmetry have not been answered yet. Beyond the Standard Model, new physics or alternatives to the Standard Model may be discovered. This includes possible indication for supersymmetry or extra dimensions which may become tangible at the TeV scale. Additionally, comprehensive studies of QCD, electroweak, and flavor physics are carried out at the LHC. [4]

2.2 The CMS Experiment

The Compact Muon Selenoid (CMS) experiment is one of the two large general purpose detectors at the LHC and it is capable of investigating an extensive range of physics. One of the main goals of this experiment was to discover the Higgs boson [4]. Depending on the Higgs mass, different decay channels are best suited for detection. In the vicinity of a Higgs mass at $114\,\mathrm{MeV/c^2}$, the lower Higgs mass limit as determined by the LEP experiment in 2003 [18], Higgs to $\gamma\gamma$ or Higgs to ZZ were the most promising channels which require supreme detection sensitivity and high energy resolution of photons and charged leptons [4]. Other channels used for discovery such as Higgs to $b\bar{b}$ and Higgs to $\tau^+\tau^-$ are challenged by the large QCD backgrounds, which can be reduced by efficient b-tagging and τ reconstruction.

The CMS experiment was designed to meet these requirements. It comprises of a high field (4 T) superconducting solenoid magnet. The bore of the solenoid is large enough to embed the tracking detector (innermost part), electromagnetic calorimeter and hadronic calorimeter. Consequently, momentum and energy of charged leptons can be measured precisely without losses due to crossing of the coil. Outside the magnet muon chambers are located within the return yoke of the magnet, providing accurate muon measurements. The detector further possesses a hermetic geometric coverage around the beam interaction point [4].

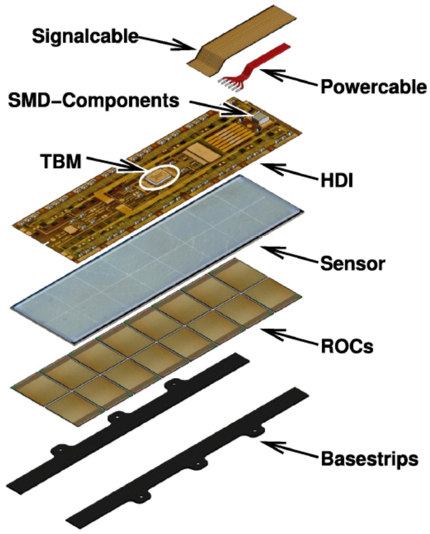

Figure 1: Exploded view of a full module as used in the pixel barrel detector [6].

2.3 The CMS Pixel Barrel Detector

The CMS tracking detector consists of a barrel and two endcaps. In the barrel region the innermost tracker part consists of three layers of pixel detectors (radii $4.4 - 10.2\,\mathrm{cm}$) followed by silicon micro strip detectors (radii $20 - 110\,\mathrm{cm}$). Due to a high track density in the region closest to the interaction point, the first layers of the tracker were chosen to consist of pixels in order to provide high granularity for 3D hit position reconstruction, which is used as seed for track reconstruction in the outer silicon micro strip detectors or muon chambers. Additionally, the pixel detector provides information for the reconstruction of secondary vertices originating from long living particles.

The spacial resolution is significantly influenced by charge sharing between pixels due to Lorentz drift in the magnetic field. The resolution amounts to $10\,\mu\mathrm{m}$ in the $r\phi$-plane and $20\,\mu\mathrm{m}$ along the beam axis while having pixels of the size of $100\,\mu\mathrm{m} \times 150\,\mu\mathrm{m}$[4].

The pixel sensors [6] are realized in a n-in-n technology, i.e a highly doped n-implant on a low n-doped bulk on the sensor front side. A p-doped implant is placed on the back side. This design implies the read out of electrons. After irradiation “type-inversion” occurs in the bulk, as explained in sec. 3. The sensors are $285\,\mu\mathrm{m}$ thick and require bias voltage of $50-60\,\mathrm{V}$ for full depletion. The operational voltage of non-irradiated sensors is $150\,\mathrm{V}$, yielding over-depletion.

Fig. 1 shows an exploded view of a detector module. Each pixel contains a sensor which is bump-bonded to a Pixel Unit Cell (PUC). The PUC handles the signal amplification and sampling. On one ROC the pixels are arranged in 52 columns and 80 rows. The ROC can be adjusted by numerous DACs [1]. Sixteen ROCs are combined in one module and controlled by the Token Bit Manager (TBM). The TBM is connected to the ROCs on a module via the

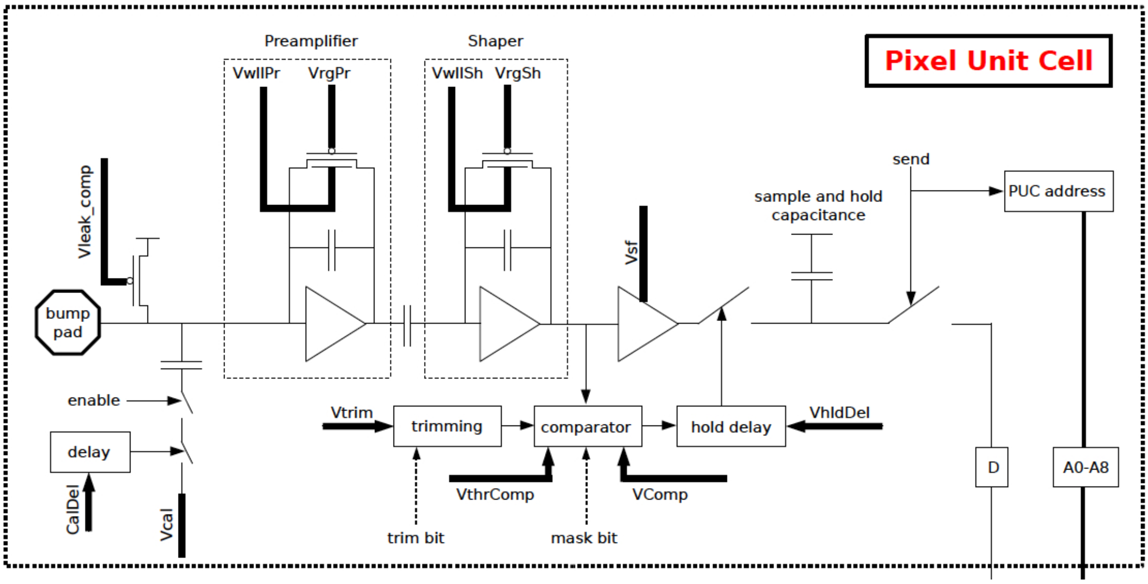

Figure 2: Schematic view of the readout chain of a Pixel Unit Cell (PUC). The sensor is connected to the PUC via a bump pad [1].

High Density Interconnect (HDI). The ROCs buffer the signals until they are read on request of the TBM.

In fig. 2 the readout chain of a PUC is shown. The signal path is briefly described as follows: A signal can either be induced from the sensor which is connected via the bump pad or from the internal calibration signal *Vcal* via a capacitance. First, the signal goes through the preamplifier and shaper. Next, the comparator determines whether the signal is sampled and stored in the sample and hold capacitor. The threshold of the comparator is adjusted for the whole ROC by *VthrComp* DAC and can be lowered in each pixel independently using trim bits and the *Vtrim* DAC. Subsequently, the signal is forwarded to the double column periphery (two columns share one periphery) where it is buffered. The relevant DACs and their function in the context of this thesis are listed in the appendix.

3 Irradiation Effects on Semiconductors and Electronic Devices

The following section describes the irradiation effects on semiconductors and electronics which have impact on the sensor and readout chip properties.

3.1 Irradiation Environment of the CMS Pixel Detector

Being adjacent to the beam interaction point, the pixel detector is exposed to high fluences. The innermost layer of the pixel detector is irradiated with about $3 \times 10^{14}\,\mathrm{n}_{eq}/\mathrm{cm}^2/\mathrm{yr}$ at

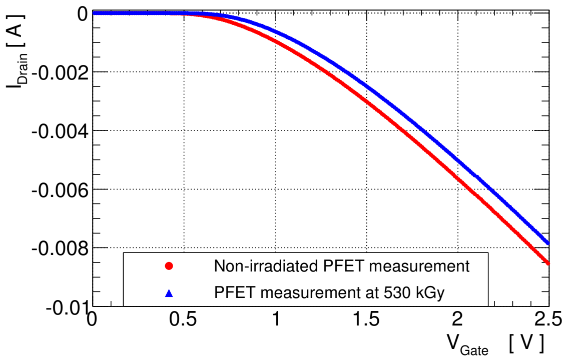

(a)

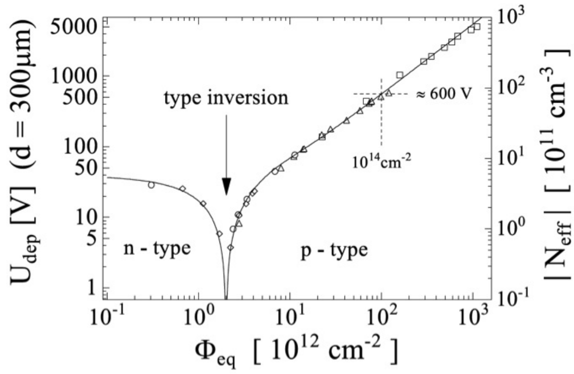

(b)

Figure 3: (a) Example of the influence of irradiation on the IV-curve of a p-type MOSFET. After irradiation, the threshold gate voltage increases [12]. It should be noted that the *Vtrim* DAC is based on a PFET and will therefore also experience a shift due to irradiation.
(b) Irradiation dependence of the effective doping concentration N_{eff} and full depletion voltage U_{dep} for a 300 µm thick sensor. For high irradiation a "type-inversion" of the bulk material is observed [21].

full LHC design luminosity ($10^{34}\,\mathrm{cm}^{-2}\mathrm{s}^{-1}$) [4] and it is designed to withstand irradiation of $6 \times 10^{14}\,\mathrm{n}_{eq}/\mathrm{cm}^2$ corresponding to two years of operation at full luminosity [19].

3.2 Interaction of Radiation with Semiconductors

Irradiation can cause defects in semiconductors which alter its electric properties. Most important are crystal defects in silicon (the bulk) and the surface defects at the Si-SiO_2 interface which are described in the following [14, 17].

Bulk Defects: Bulk defects consist of displaced silicon atoms in the lattice [14, 17]. Displacement is caused by nuclear scattering processes with incident or secondary heavy particles such as neutrons, protons or pions and can occur as point defects or in clusters. In order to compare the damage caused by different radiation types, the radiation damage is scaled to non-ionizing-energy-losses (NIEL). The displacement results in creation of new interstitials and vacancies in the crystal, which are mobile, and which can form stable defects such as phosphorous-vacancy or oxygen-vacancy complexes. Defects create energy levels in the semiconductor band gap contributing to the leakage current. The defect levels can also have charged states and can alter the space charge concentration of the bulk. Deep level defects can cause resistivity increase in non-depleted bulk regions. In addition, defect levels can "trap" free charge carriers for timespans of the order of micro seconds, which is beyond the charge collection time in a semiconductor sensor.

Defects at the Si-SiO$_2$ Interface: Radiation damage to oxides in the Si-SiO$_2$ interface is caused by ionization through charged particles [14]. Oxides have a highly irregular structure, in which electron mobility exceeds hole mobility, and can be considered as trapping centers. As a consequence of mobility differences, cumulative ionization leads to a net amount of positively charged oxide trapped holes at the interface. In the presence of an electric field, such as in MOS transistors, oxide trapped holes can accumulate at the Si-SiO$_2$ interface. A shift of the MOS flat band voltage can be observed leading to shifts of threshold voltages, as shown in fig. 3a [2, 12].

Yet another contribution of defects may arise from trivalent silicon atoms with dangling bonds [17]. Ionization can cause chemical bond rupture and thus further negatively or positively charged interface states. Atomic displacement can be neglected as a source of defects in oxides, since a highly irregular structure already exists [2].

3.3 Consequences of Irradiation Effects on CMS Sensors and Readout Chip

Based on the previously discussed microscopic effects of radiation interaction with semiconductors, changes of electrical properties of electronic devices can be observed. These changes are discussed in the following in the context of the CMS pixel sensor and readout chip.

Consequences for Sensors: As sensors have only low doping concentrations, defects caused by irradiation have large impact on the sensor behavior. Mainly three effects are important for irradiated sensors. First, changes in the space charge density affect the field distribution. Higher bias voltages (up to 600 V) are required for over-depletion. In fig. 3b the effective doping concentration N_{eff} as well as the required bias voltage for full depletion is shown as a function of equivalent neutron fluence. For high irradiation a "type-inversion" of the bulk doping concentration is observed. A second important effect is the increase of leakage currents due to additional generation and recombination centers. Generation and recombination in a semiconductors denote the processes in which mobile charge carriers are created or removed. The presence of such center further influences the shape of the electric field [17]. Thirdly, trapping results in a decreased mean free path of signal electrons [17].

Consequences for Electronic Components: As already mentioned in sec. 3.2, surface defects occurring in the Si-SiO$_2$ interface affect the insulator field of MOS transistors. Due to the high doping concentration, which is an intrinsic feature of semiconductor based electronics, change of space charge concentration can be neglected in electronic components [17]. In MOS transistors, the buildup of interface states leads to different working points, e.g. higher threshold voltages. An example can be seen in fig. 3b for a p-type MOSFET transistor [12]. The irradiation induced threshold change affects for instance the *Vtrim* DAC which is realized with a p-type MOSFET (PFET) [13]. Interface states also lead to the decrease of surface carrier mobility and hence to a reduced transconductance. Further, parasitic current channels might develop due to surface defects. In total, such defects change the working points of amplifiers, DACs and other components on the readout chip.

Shift of the Band Gap Reference Voltage: One of the consequences of irradiation of the readout chip is the shift of the band gap reference voltage V_{ref} [9]. The band gap reference voltage V_{ref} serves as reference voltage for all internal voltages on the chip. Therefore, DACs such as *Vcal* are affected by an irradiation induced change of V_{ref}. Previous studies observed a rise of V_{ref} (see appendix). Therefore the voltages of e.g. *Vcal* or other DACs are expected to rise.

4 Methods, Setup and Samples

This section lays out the experimental methods and techniques used for the measurements of irradiation effects on the analog and digital pixel readout chip, which are presented in sec. 5. The methods are implemented using the software package *psi46expert* for communication with the *PSI46* test board. Unless explicitly mentioned, the presented methods apply to analog as well as digital chips.

4.1 Vtrim – Investigation Methods

In order to adjust the thresholds of all pixels in one ROC to the same value, the 8 bit *Vtrim* DAC is used. *Vtrim* defines the range of the trim bits which are used to lower the global comparator threshold (set by *VthrComp*) during the so called trimming procedure. Trimming yields the threshold unification to one specified *Vcal* value (see details in [20]). Thus, for examining the influence of irradiation on *Vtrim*, the comparator threshold distribution of all pixels in one ROC has to be measured as a function of *Vtrim*. During this test all trim bits are enabled[2]. An example of the threshold reduction is shown in fig. 4.

The threshold can be obtained in two ways, either by measuring the "*Vcal*-threshold" or the "*VthrComp*-threshold". The former consists of measuring the response efficiency for rising *Vcal* for a fixed comparator threshold value (i.e. *VthrComp*). The threshold is given as the value, for which the response efficiency reaches 50%. The latter instance works by setting the internal calibration signal *Vcal* to a fixed value and reducing the threshold by increasing *VthrComp*[3] until the response efficiency reaches 50% [3]. For the measurement within this thesis, the *Vcal*-threshold method has been used, giving a threshold in terms of *Vcal* units.

[2] The 4 bit trim bits determine the fraction of *Vtrim* by which the threshold is lowered. For disabled trim bits the threshold is not lowered while for fully enabled trim bits the threshold is decreased with the full *Vtrim* amplitude.

[3] Increasing *VthrComp* on the ROC is actually decreasing the physical comparator threshold since the *VthrComp* DAC is inverted.

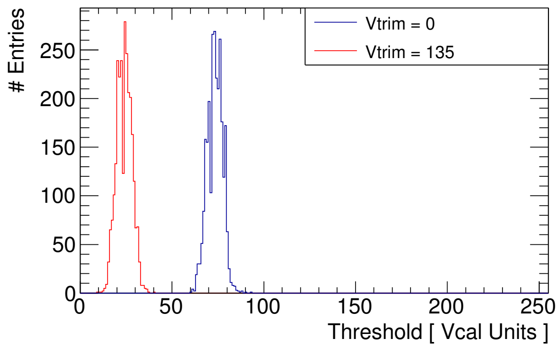

Figure 4: Example of a comparator threshold reduction using two different *Vtrim* values for a non-irradiated analog ROC.

Due to the different raising time of high and low amplitude signals, the thresholds measured in the triggered bunch crossing[4] and in the subsequent one are different.The absolute threshold, also called timing independent threshold, is defined as the minimum threshold measured for different bunch crossing [20]. In contrast, the in-time threshold only considers signals in one fixed bunch crossing. As signals with low amplitude could exceed the comparator threshold in another bunch crossing, the in-time threshold does not hold as absolute scale. Therefore, the absolute threshold method has been used for determination to the *Vcal*-threshold.

4.2 Pulse Height – DAC Optimization Procedure

Pulse height DAC optimization has been carried out for the digital *PSI46digV2* chip. The optimization aims at enhancing the performance of the pulse height calibration by achieving linearity of the pulse height with respect to the internal calibration signal in the low *Vcal* range, and by achieving usage of the entire available pulse height range.

Photon energies of the order of keV, as used during the calibration with X-rays, generate pulse heights in the low *Vcal* range. Optimal range usage is especially important for the digital chip, since its output range is rather limited compared to the range of the ADC output of the analog *PSI46V2* chip. However, a temperature dependence of the pulse height requires to leave a margin of 30 pulse height DAC units at the lower end, when optimizing at 17°C. Otherwise, the pulse height would shift out of bound in the low range at −20°C.

Only four out of 22 DACs[5] on the ROC have been used in the DAC optimization procedure. In a first step, the pulse height was shifted vertically by *VoffsetRO* DAC. The DAC *IBias_DAC* was used to stretch or squeeze the pulse height in vertical direction. In a second step, the linearity in the low *Vcal* range was optimized by the *Vsf* DAC. Iterations of those

[4] Similar to the real operating conditions at LHC, different bunch crossings can be triggered for readout of the internal calibration signals.

[5] The digital ROC has fewer DACs than the analog one, which has 26 DACs.

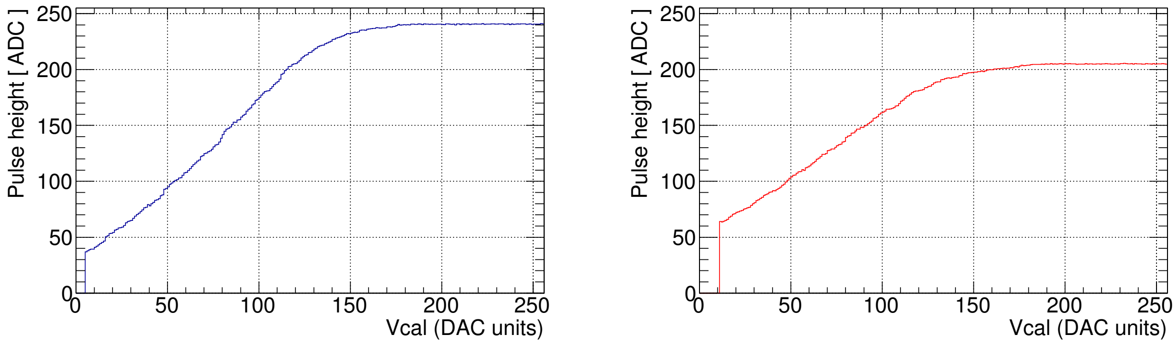

(a) (b)

Figure 5: Example of DAC optimization: The pulse height versus *Vcal* is shown in the high *Vcal* range for one pixel. Figure (a) shows an optimized DAC setting making use of the available pulse height range. Linearity in the low *Vcal* range is given (but cannot be seen on this scale). Figure (b) displays a non-optimized pulse hight.

two steps resulted in an optimized pulse height. An example of DAC optimization is shown in fig. 5a and fig. 5b.

4.3 Vcal Calibration – Spectrum Method

The calibration of the internal calibrate signal *Vcal* can be performed using monochromatic X-rays. The objective of the calibration is to determine the equivalent of one *Vcal* unit in electrons. Hence, any change of ROC properties on e.g. comparator threshold, *Vtrim* DAC or other, could be translated into electrons providing an absolute scale of irradiation effects.

The calibration procedure is carried out in three steps: First, the ROC is trimmed (see explanation in previous sec.). Secondly, the pulse height of all pixel is calibrated in terms of *Vcal* units [3]. The pulse height DAC optimization ensures a linear dependence in the relevant low *Vcal* range. Third, monochromatic X-rays are injected into the sensors. Each photon creates $\mathrm{N} = \mathrm{E}_{K_\alpha}/3.6\,\mathrm{eV}$ electrons which are to be read out. K_α denotes the emission line from which the X-rays originate. The resulting pulse height can be translated into *Vcal* units using the second step. Due to linearity of the pulse height, the entire low *Vcal* range can be calibrated with at least two different X-ray energies. This procedure is known as spectrum-method.

4.4 Vcal Calibration – Trim-Threshold-Method

The trim-threshold-method has been developed as an alternative to the spectrum-method (see previous section) and the existing threshold-method. In the first step of this method, the entire ROC is trimmed to several different *Vcal* values. Then, for each trim value, the number of hits from X-ray irradiation is determined, yielding an S-Curve with an additional linear

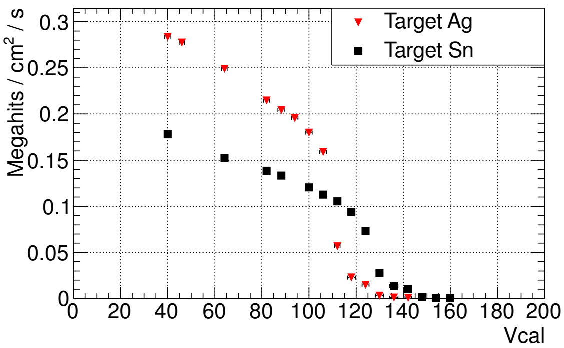

Figure 6: Example of the trim-threshold-method for a non-irradiated ROC for X-rays originating from a silver and a tin target.

part as output. The *Vcal* value to which the number of hits amount to 50% of the maximum number of hits corresponds to the respective monochromatic X-ray energy.

In contrast to the already existing threshold-method, the trim-threshold-method ensures that all pixel have the same threshold. This method has been used to show the impact of trapping on the sensor output. An example is given for a non-irradiated analog chip in fig. 6.

4.5 Vcal Calibration – Band Gap Reference Voltage Method

For irradiated chips an alternative method has been developed which is independent of irradiation defects in the sensor. The method is based on the band gap reference voltage V_{ref} which serves as reference for all internal voltages. V_{ref} shifts upon irradiation and is therefore responsible for a shift of the *Vcal* DAC which ultimately results in a different *Vcal* calibration slope [13].

The internal calibration signal is created by inducing a charge Q on a capacitor C using the *Vcal* DAC (see fig. 2). The *Vcal* DAC on the other hand depends on V_{ref}. Q can be parametrized with a slope and offset in electrons or can be expressed with the capacitance C and a fraction f of V_{ref}, where f is determined by the *Vcal* DAC

$$\mathrm{Q} = \mathrm{slope} \cdot Vcal + \mathrm{Offset} = \mathrm{C} \cdot \mathrm{f} \cdot V_{ref}\,. \tag{1}$$

Based on the assumption that C does not change with irradiation (C consists of metal plates and glass dielectric (SiO_2) and is therefore not prone to defects [16]), only a change $\delta V_{ref}/V_{ref}\ (\phi)$ (the relative increase of V_{ref} depending on irradiation fluence) can alter the induced charge

$$\mathrm{Q}_{\,\mathrm{Irrad}} = \left(1 + \frac{\delta V_{ref}}{V_{ref}}\ (\phi)\right) \cdot \mathrm{Q}_{\,\mathrm{Non\text{-}Irrad}}\,. \tag{2}$$

However, V_{ref} is not directly accessible on the readout chip. Instead other voltages depending on V_{ref} can be measured, in order to reconstruct the relative band gap reference voltage shift

$\delta V_{ref}/V_{ref}$ and thus the new calibration slope. One of such voltages is $Vdig$, which can be measured as a function of the $Vdig$ DAC. One finds [13]

$$Vdig\,(Vdig\ \mathrm{DAC})_{\,\mathrm{Irrad}} = \left(1 + \frac{\delta V_{ref}}{V_{ref}}\,(\phi)\right) \cdot Vdig\,(Vdig\ \mathrm{DAC})_{\,\mathrm{Non\text{-}Irrad}}\ . \tag{3}$$

Having determined $\delta V_{ref}/V_{ref}\ (\phi)$, the new slope after irradiation can be finally determined based on the slope of non-irradiated chips

$$\mathrm{slope}_{\,\mathrm{Irrad}} = \left(1 + \frac{\delta V_{ref}}{V_{ref}}\,(\phi)\right) \cdot \mathrm{slope}_{\,\mathrm{Non\text{-}Irrad}}\ . \tag{4}$$

As reference slope the value of 65 ± 9 electrons per $Vcal$ (obtained for a large sample of chips [20]) is used for the analog sample since the slopes have not been determined before irradiation. For the digital sample the slope before irradiation has been determined.

4.6 Experimental Setup and Samples

X-ray Irradiation Setup: The X-ray irradiation setup used for $Vcal$ calibration consists of a X-ray tube and a selection of targets, i.e. Fe, Cu, Br, Mo, Ag, Sn and Ba. As listed in tab. 1, the targets have different energies of the characteristic emission line K_α. The interaction cross section of photons with keV energy is mainly determined by the photo-electric effect and decreases with increasing energy [10, 15].

Target	E_{K_α}	N_{el}
Fe	6404.0062	1779
Cu	8047.8227	2235
Br	11924.36	3312
Mo	17479.372	4855
Ag	22162.917	6156
Sn	25271.36	7019
Ba	32193.262	8942

Table 1: Targets and corresponding energy of K_α transition line [15], as well as number of created electrons used for $Vcal$ Calibration.

Cooling: Cooling of chips has been carried out as irradiated chips have large leakage currents due to radiation damage in the sensor and electronic components (see sec. 3.3). A cooling box has been used for the measurement, containing water cooled peltier elements and dry air supply for humidity control. All measurements have been performed at minus 10 °C.

Irradiation Conditions: The digital sample was irradiated at the proton irradiation facility at Karlsruhe Institut for Technology (KIT). During irradiation two third of the chips in the sample have been powered. This implies that bias voltages are applied to electronic components which might influence the creation and annealing of irradiation defects. The analog sample was irradiated at KIT in 2011 without being powered.

Samples: Within this thesis, analog *PSI46V2* chips and digital *PSI46digV2* chips have been investigated. Two analog samples were used, one with irradiated sensors and ROCs and the other with irradiated ROCs and non-irradiated sensors. The first analog sample has been irradiated to $4.2 \times 10^{14}\,\mathrm{n_{eq}/cm^2}$ (1 chip), $6.1 \times 10^{14}\,\mathrm{n_{eq}/cm^2}$ (2 chips), $1.1 \times 10^{15}\,\mathrm{n_{eq}/cm^2}$ (2 chips), $1.5 \times 10^{15}\,\mathrm{n_{eq}/cm^2}$ (2 chips) and $3 \times 10^{15}\,\mathrm{n_{eq}/cm^2}$ (2 chips). One non-irradiated chip completed the sample.

The second analog sample consisting of ROCs with non-irradiated sensors was irradiated to $3 \times 10^{14}\,\mathrm{n_{eq}/cm^2}$, $6 \times 10^{14}\,\mathrm{n_{eq}/cm^2}$ and $1.1 \times 10^{15}\,\mathrm{n_{eq}/cm^2}$. Afterwards the sensors have been attached. The bump bonding procedure includes a heating step to 200 °C and annealing might have occurred. For this reason, one ROC has been tested before and after sensor attachment. In particular the *Vtrim* influence on the *Vcal* threshold is able to reveal changes of the irradiation effects, but no noticeable effects of the heating procedure have been observed.

The digital sample consisted of 21 chips of which 15 chips were irradiated with $6 \times 10^{14}\,\mathrm{n_{eq}/cm^2}$ at KIT. Finally, it is assumed that all fluences have an uncertainty of 10 %.

5 Measurements and Results

In the following the measurements and results are presented for investigation of irradiation effects on the analog and digital chip. Based on the methods presented in the previous section, the calibration results are first described, followed by the irradiation effects on *Vtrim*. Each section is concluded with a discussion of the results.

5.1 Analog Chip – Vcal Calibration after Irradiation

The commonly used calibration procedure for ROCs or modules of the pixel detector is the spectrum method. In the following this method, as well as the new developed band gap reference voltage calibration method are examined for irradiated ROCs.

Vcal Calibration using the Spectrum Method: For irradiated analog chips the spectrum method returned unreasonable results. Very high slopes (up to 300 electrons per *Vcal* unit) were obtained for irradiated chips which is shown exemplary in fig. 7a. It was further observed that on the one hand the number of detected hits decreased, while on the other hand the characteristic shapes of the spectra changed, which is exemplary shown in fig. 7b. Optimization of DACs such as *Vana* (providing power to the pixels) or *VholdDel* (adjusting the sample and

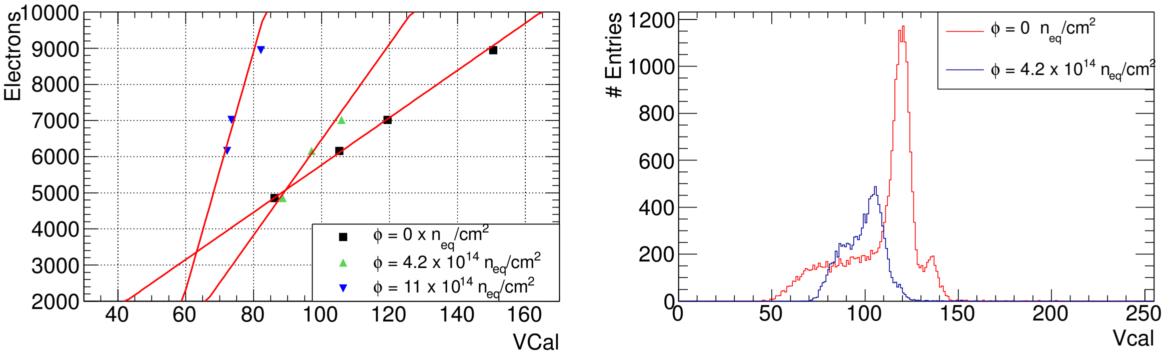

(a) (b)

Figure 7: (a) Exemplary results for the calibration slope of a non-irradiated chip and two irradiated ones. The non-irradiated chip returns the expected slope of 65 electrons per *Vcal*. For the fluence of $11 \times 10^{14}\,\mathrm{n_{eq}/cm^2}$ a slope of 330 electrons per *Vcal* is obtained.
(b) *Vcal* spectrum of monochromatic X-rays originating from the K_α line of tin for a non-irradiated chip and an irradiated one. The bias voltage was set to $-600\,\mathrm{V}$ for the irradiated chip. Nevertheless fewer hits are observed for the irradiated Chip.

hold DAC) could not increase the detected number of hits or restore the original spectrum shapes.

The trim-threshold-method (see sec. 4.4) was subsequently used to investigate the origin of the decrease of number of detected hits. Measurements using this method are shown in fig. 8a for two different bias voltages. Having a bias voltage of $-150\,\mathrm{V}$, no characteristic S-curve is visible. This implies that the signal loss of irradiated ROCs occurs before the signal passes the comparator, i.e. in the sensor, preamplifier or shaper. Adjustments of the shaper *VwllSh* and preamplifier *VwllPr* feedback DACs could not raise the number of hits. The reason for the signal loss was thus identified as loss due to irradiation defects in the sensor (see sec. 3.3). Two irradiation defects seem to be most important: First, trapping reduces the charge collection efficiency and second, a change of the effective doping concentration reduces the depletion field and therefore the statistics since charge is only collected when being created in the drift field.

In fig. 8b the dependence of detected hits on the bias voltage is shown. The higher the bias voltage the more hits are detected since the depletion field is further extended into the bulk and since the charge collection time rises, resulting in less trapping. However a saturation is not reached yet.

For an increased bias voltage of $-600\,\mathrm{V}$ the characteristic S-curve becomes visible. However, calibration of the lowest irradiated chip in the sample (fluence $4.2 \times 10^{14}\,\mathrm{n_{eq}/cm^2}$) still resulted in a slope of 97 electrons per *Vcal* unit which is a lot higher than the reference value (non-

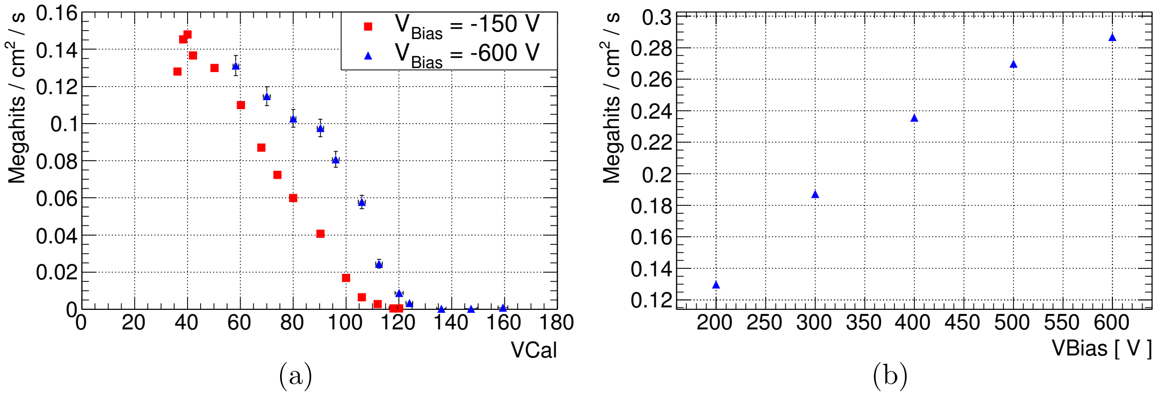

Figure 8: (a) Results obtained using the trim-threshold-method (see sec. 4.4) for a chip with irradiation to $4.2 \times 10^{14}\,\mathrm{n_{eq}/cm^2}$ and use of monochromatic X-rays from a tin target. For bias voltage of 150 V most of the hits occur for low *Vcal* values. This implies signal loss due to irradiation defects in the sensor. For bias voltage of -600 V more hits can be detected, since the depletion field extends deeper into the bulk. Also the charge collection is increased yielding less charge trapping.
(b) Number of hits vs. bias voltage for an irradiated chip (fluence $4.2 \times 10^{14}\,\mathrm{n_{eq}/cm^2}$).

irradiated chip, [20]) of 65 electrons per *Vcal*. This implies that irradiation defects in the sensor still remain a problem for the calibration.

Vcal Calibration using the Relative Band Gap Reference Voltage Method: The shift of the band gap reference voltage V_{ref} is the actual reason for the change of the calibration slope after irradiation since V_{ref} serves as reference voltage for all internal voltages. As the calibration based on the spectrum method is deteriorated by irradiation defects in the sensor (see previous section), the relative band gap reference shift has been investigated.

The relative band gap reference shift $\delta V_{\mathrm{ref}}/V_{\mathrm{ref}}$ has been determined using the voltage *Vdig* as a function of *Vdig* DAC. The method and analysis are explained in sec. 4.5. For the analog chip the analysis was based on data from [9] (see appendix).

Fig. 9a shows the relative band gap reference shift $\delta V_{\mathrm{ref}}/V_{\mathrm{ref}}$ as a function of increasing irradiation fluence. For each fluence a sample consisting of several chips has been analyzed. One observes that $\delta V_{\mathrm{ref}}/V_{\mathrm{ref}}$ shifts already after the first irradiation step by 8%. The results are in line with previous studies on the band gap reference voltage [12, 13] (see appendix).

The results shown in fig. 9a were used to obtain the *Vcal* calibration slope presented in fig. 9b. The slopes correspond to the reference slope times the value of $(1 + \delta V_{\mathrm{ref}}/V_{\mathrm{ref}})$ for the respective fluence (see sec. 4.5). The slope seems to plateau at 72 electrons per *Vcal*.

Vcal Calibration of Chips with Irradiated ROCs and Non-irradiated Sensors: In order to obtain the *Vcal* calibration slope using the spectrum method with X-rays, non-irradiated

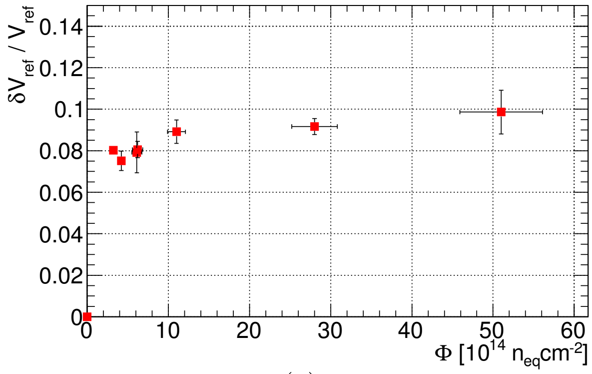

(a)

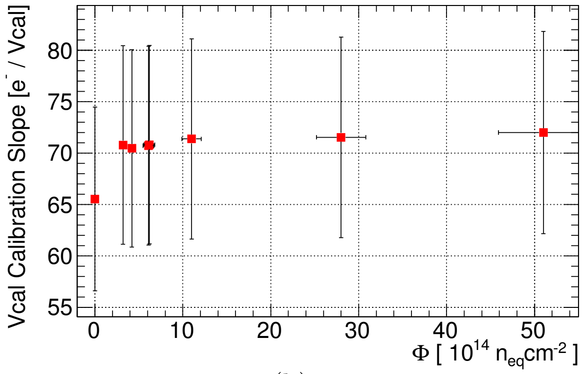

(b)

Figure 9: (a) Relative change of the band gap reference voltage V_{ref} based on the data from [9]. V_{ref} increases up to 10% with respect to non-irradiated reference voltages. A saturation seems to occur at high fluence.
(b) Slope in electrons per *Vcal* DAC unit for analog chips as a function of irradiation. The slope has been obtained based on the relative change of the band gap reference voltage (a). The large errors of the *Vcal* calibration arise from the large uncertainty on the calibration slope of non-irradiated ROC, which is taken from [20] (see sec. 4.5).

sensors were bump-bonded to irradiated ROCs. Fig. 10 shows the resulting calibration slope in electrons per *Vcal*. For comparison the results of the calibration slope from the relative band gap measurement (fig. 9) are shown as reference values.

The calibration results using irradiated ROCs and non-irradiated sensors are in line with the calibration results obtained using the relative band gap reference voltage method. The calibration slopes seem to plateau at a value of 70 electrons per *Vcal*. Using non-irradiated sensors the measured *Vcal* spectra of the different X-ray targets (tab. 1) resemble the spectra of completely non-irradiated chips.

Discussion of the Results: The measurements reveal that the calibration based on the spectrum method with X-rays is deteriorated. Bulk defects that cause trapping reduce the charge collection efficiency and therefore the pulse height. Hence, the calibration procedure, which relies on matching the pulse height created by the internal calibration signal *Vcal* with the pulse height from a known energy deposition, is not viable. Additionally, changes of the effective doping concentration reduce the depletion field in the sensor which results in lower statistics.

In contrast, the new calibration method based on the band gap reference voltage gives promising results which are confirmed by the calibration results of irradiated ROCs with non-irradiated sensors. The band gap reference voltage shift implies that a 10% change of the calibration slope is expected for the highest tested irradiation fluence.

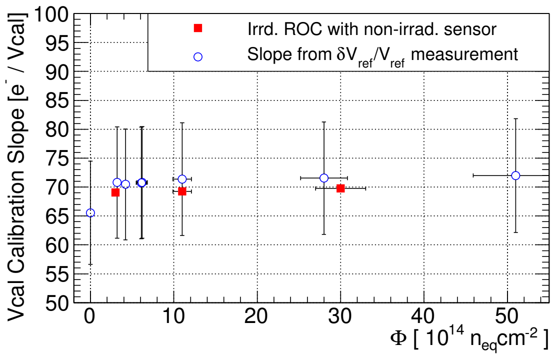

Figure 10: The slope in electrons obtained from *Vcal* calibration with X-rays is shown for increasing irradiation. The results from fig. 9 are shown for comparison. Both measurements seem to be in agreement.

In conclusion, the spectrum method should not be used for irradiated chips without further investigations of the charge collection efficiency. The method based on the band gap reference voltage seems to be reliable for calibration.

5.2 Analog Chip – Irradiation Effects on Vtrim

In order to study irradiation effects on the *Vtrim* DAC, the influence of this DAC on the comparator threshold has to be analyzed. In this regard several different properties can be examined.

The first property to investigate is how much *Vtrim* can reduce the comparator threshold for different irradiation fluences and whether this is still sufficient for the trimming procedure. Trimming can be performed succesfully as long as the threshold spread between the pixels is smaller than the maximum threshold reduction using the *Vtrim* DAC. A second property to investigate is at what value *Vtrim* starts to reduce the threshold and whether this "*Vtrim* threshold" is irradiation dependent.

Based on measured and linearly interpolated *Vcal* calibration data from irradiated ROCs with non-irradiated sensors (fig.10) the investigated properties can be futher expressed in terms of electrons. In addition *Vtrim* can be stated in terms of electrons per DAC unit.

Measurements and Results: The mean *Vcal* threshold per ROC as a function of *Vtrim* is presented in fig. 11a for different irradiation fluences. The analyzed properties of fig. 11a are shown in the adjoining figures.

Fig. 11b shows the $5\,\sigma$ spread of the comparator threshold distributions in *Vcal* units versus irradiation. The higher the irradiation the larger becomes the threshold spread. The dependence of *Vtrim* threshold on irradiation is presented in fig. 11c. Here, the *Vtrim* threshold is defined as the *Vtrim* value, for which comparator threshold is decreased by 5%. One observes that the higher the irradiation the higher is the *Vtrim* threshold. In fig. 11d the maximum threshold reduction is shown in terms of *Vcal* units and in fig. 11e in terms of electrons. One observes that *Vtrim* becomes less effective for increasing fluence. Finally the calibration slope of *Vtrim* in terms of electrons per DAC is displayed in fig. 11f. It is defined as

$$\mathrm{slope}_{\mathrm{Vtrim}} = \Delta y_{\mathrm{max}}(\phi)/\Delta\, Vtrim_{\mathrm{lin}}(\phi) \;, \tag{5}$$

where $\Delta y_{\mathrm{max}}(\phi)$ denotes the maximum threshold reduction in electrons as shown in fig. 11e and $\Delta\, Vtrim_{\mathrm{lin}}(\phi)$ denotes the length of the linear region.

Discussion of the Results: *Vtrim* shows a strong dependence on irradiation. As the *Vtrim* DAC is based on a PFET, it is affected by the PFET threshold voltage shift upon irradiation as presented in fig. 3b. The higher the fluence the higher must be the gate voltage of a PFET in order to reach the same drain current. For this reason the *Vtrim* threshold increase is observed, as well as a reduction of the impact of *Vtrim* on the comparator threshold. With respect to the trimming procedure, it can be further observed that the possible threshold reduction using *Vtrim* is not sufficient anymore for the highest irradiation fluence of $6 \times 10^{14}\,\mathrm{n}_{\mathrm{eq}}/\mathrm{cm}^2$ due to the large threshold distribution spread.

5.3 Digital Chip – Pulse Height DAC Optimization

The DAC optimization results obtained before irradiation are shown in fig. 12 for the *Vsf*, *IBias_DAC* and *VOffsetRO* DAC. The distributions are not peaking except for *IBias_DAC*. This implies that there is not a single DAC setting which is optimized for different chips simultaneously. DAC optimization after irradiation could not be carried out within the timeframe of this thesis.

5.4 Digital Chip – Vcal Calibration before and after Irradiation

Vcal calibration has been carried out for digital chips before and after irradiation. Before irradiation a sample of 21 chips was calibrated using the spectrum method. After irradiation a sample of 15 chips was calibrated using the band gap reference voltage method due to the experiences with the calibration of irradiated analog chips (sec. 5.1).

VCal Calibration before Irradiation – Using the Spectrum Method: Fig. 13 shows the calibration slope and offset distribution in electrons per *Vcal* which has been measured before irradiation. A mean slope of 51.04 ± 2.53 electrons per *Vcal* and an offset of -916.7 ± 193 electrons per *Vcal* was measured. The slope is less steep compared to the one of analog chips which amounts to 65 ± 9 electrons per *Vcal* [20].

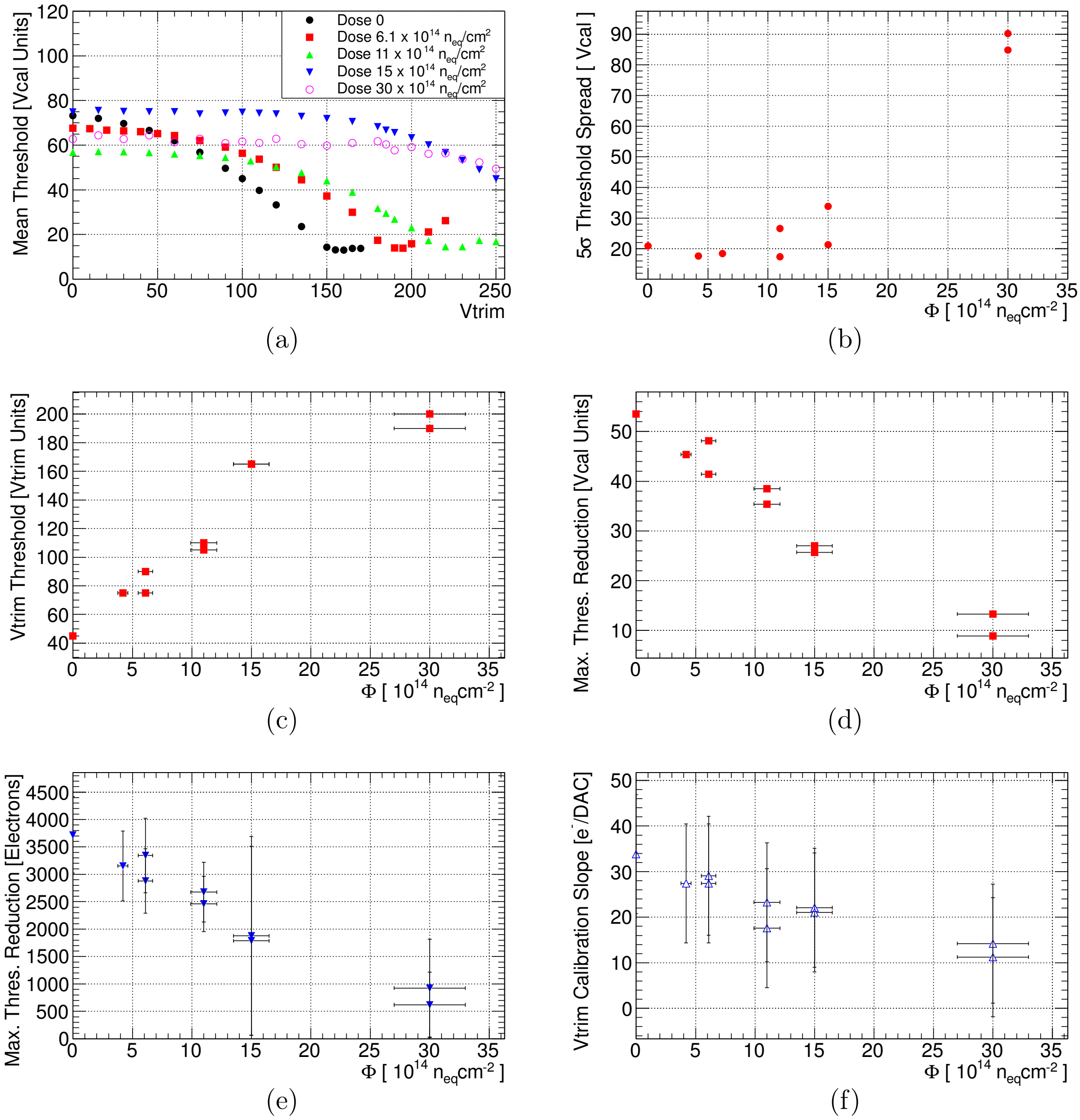

Figure 11: The mean *Vcal* threshold is shown for a selection of different irradiation levels as a function of *Vtrim* (a), the analysis of these curves includes:
(b) $5\,\sigma$ spread of the *Vcal* threshold distributions of each chip vs. irradiation.
(c) The dependence of the *"Vtrim* threshold" on irradiation fluence.
(d) The maximum threshold reduction in *Vcal* units using *Vtrim* vs. irradiation.
(e) The maximum threshold reduction in electrons using *Vtrim* vs. irradiation.
(f) The *Vtrim* calibration in electrons per *Vtrim* DAC vs. irradiation.

VCal Calibration after Irradiation – Using the Band Gap Reference Voltage Method: The calibration of the irradiated digital chips was based on the determination of the relative band gap reference shift $\delta \mathrm{V}_{\mathrm{ref}}/\mathrm{V}_{\mathrm{ref}}$ from *Vdig*. During irradiation 10 out of 15 chips of the irradiated sample have been powered. The consequences of this powering can be seen in fig. 14 which displays the measurements of the *Vdig* voltage as a function of the *Vdig* DAC before and after irradiation. For powered chips a clear distinction between the measurements before and after irradiation is observable.

Using the data shown in fig. 15, the relative band gap reference voltage shift $\delta V_{\mathrm{ref}}/V_{\mathrm{ref}}$ can be extracted. The means of the distributions are presented in fig. 15 for chips which have been powered, as well as for chips which have not been powered during irradiation. The relative shift during irradiation amounts to $3.7 \pm 2.2\,\%$ when powering the chip during irradiation and about $1.3 \pm 2.3\,\%$ when not powering the chip. The results received for the analog chips (fig. 9) are plotted as reference. One observes a smaller relative change for the digital chips in comparison to the analog chip.

Finally, the calibration slope of the irradiated digital chips was determined based on the relative band gap reference voltage shift results (fig. 15). In fig. 16 the calibration slope distributions before and after irradiation are shown for both chips which have been powered and chips which have not been powered during irradiation. Non-irradiated, the mean slope of the chips which belong to the powered sample amounts to 50.87 ± 1.62 electrons per *Vcal* and to 50.32 ± 1.11 electrons per *Vcal* for the chips in the non-powered sample. After irradiation, a small shift of the slope distribution of the powered chips is visible, yielding a mean slope of 52.54 ± 1.9 electrons per *Vcal*. The chips which have not been powered have a slope of 50.85 ± 1.96 electrons per *Vcal* after irradiation.

Discussion of the Results: The calibration of the digital sample reveals the influence of powering the chips during irradiation, as it is the case during CMS operation at LHC. It is observed that the irradiation induced shift of V_{ref} is larger when the chip was powered. This can be explained by the presence of a bias field in the electronic components such as MOS transistors. The field separates created electrons and holes, which results in a reduced recombination rate and ultimately more oxide trapped holes in the interface region [16].

5.5 Digital Chip – Vtrim Investigation before Irradiation

The dependence of the *Vcal* threshold on *Vtrim* is shown in fig. 17 for the sample of non-irradiated digital chips. In contrast to the results from the analog chips (fig. 11a) the curve is more linear. In the linear region one obtains a *Vtrim* calibration slope of 18.27 ± 1.015 electrons per *Vtrim* based on the non-irradiated calibration results. Due to the limited time of this thesis *Vtrim* on irradiated chips could not be investigated.

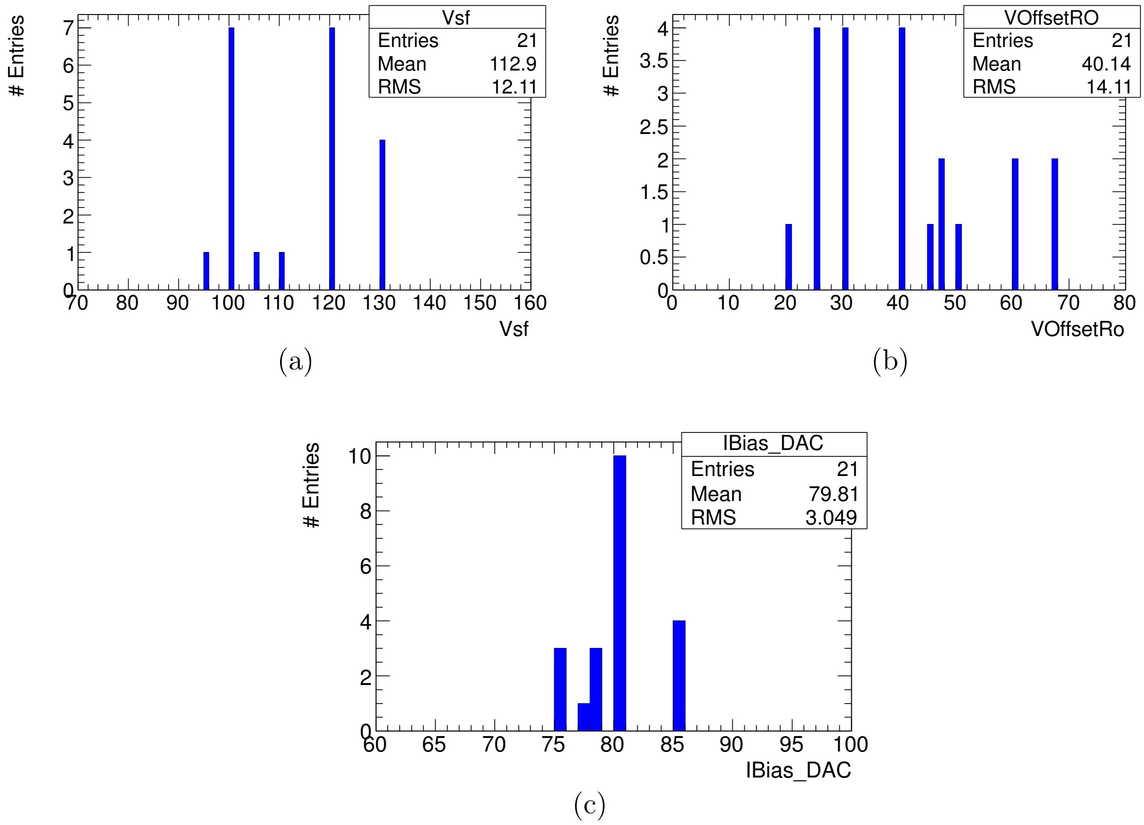

Figure 12: Parameter obtained from DAC optimization of the pulse height of digital ROCs *Vsf* DAC (a), *VoffsetRO* DAC (b), and *IBias_DAC* (c).

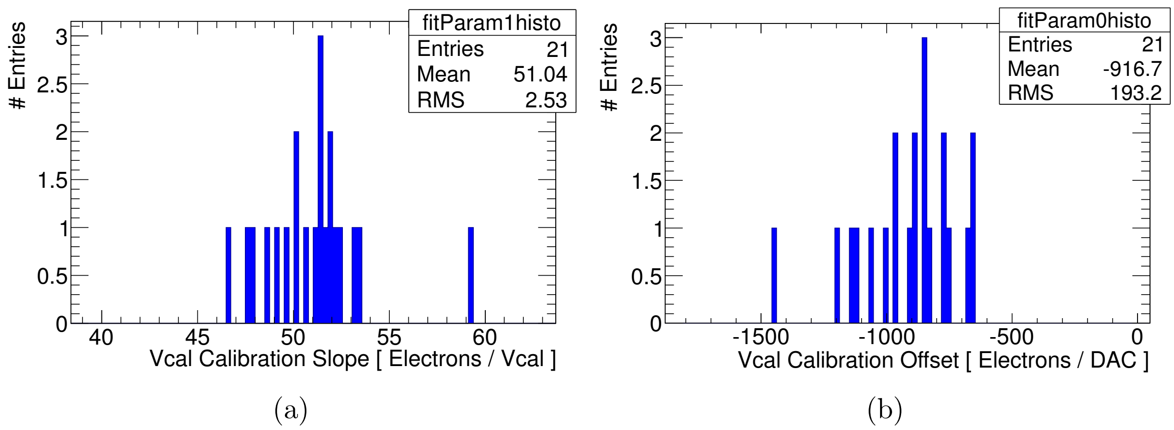

Figure 13: *Vcal* calibration results for digital chips obtained before irradiation. The mean slope is lower than the mean slope of non-irradiated analog chips which amounts to 65 ± 9 electrons per *Vcal* [20].

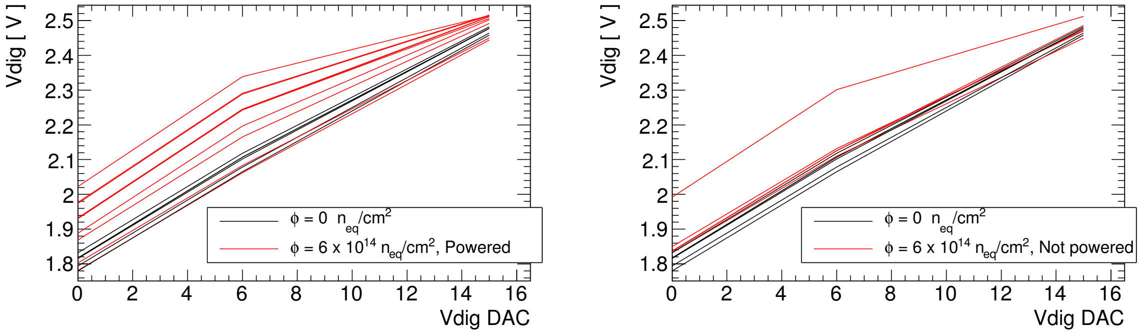

(a) (b)

Figure 14: *Vdig* voltage measurements as a function of the *Vdig* DAC. Note that the lines between the data points at *Vdig* DAC 0, 6 and 15 are drawn for visualization.
(a) The chips have been powered during irradiation. The resulting bias fields in semiconductors increases the number of oxide trapped holes and other interface states and hence promotes a band gap reference voltage shift.
(b) Chips that have not been powered during irradiation.

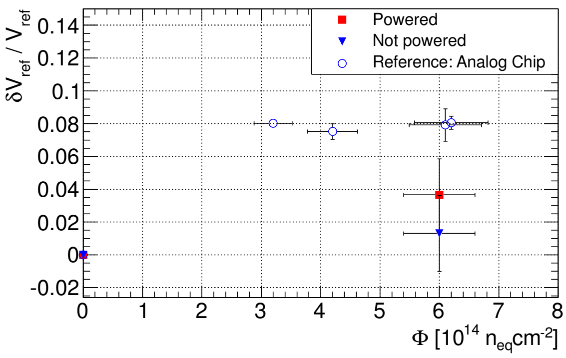

Figure 15: Relative band gap reference voltage for the digital chip with respect to irradiation. For comparison the values obtained for the analog chip (fig. 9) are plotted.

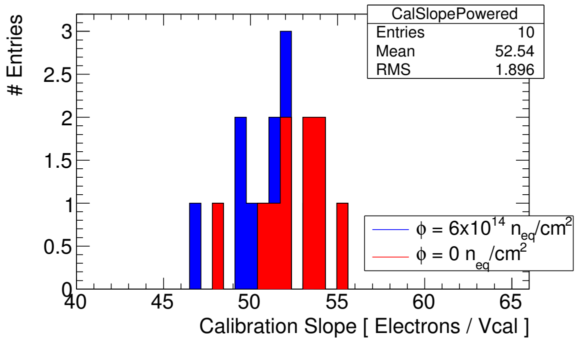

(a)

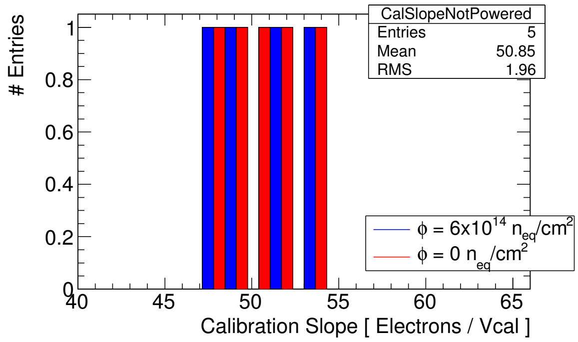

(b)

Figure 16: *Vcal* calibration results after irradiation of the digital chip based on the relative band gap reference voltage method. A part of the sample has been powered during irradiation. For these chips different irradiation slopes are measured. Additionally, the distribution for the respective non-irradiated chips is displayed. Note that the statistics box belongs to the irradiated samples. The chips which have been powered during irradiation seem to have a larger increase in slope.
(a) Chip powered during irradiation.
(b) Chip not powered during irradiation.

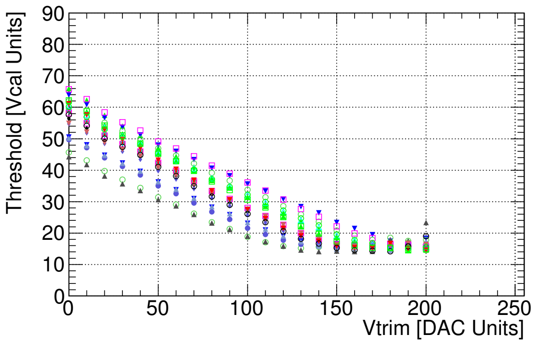

Figure 17: *Vcal* threshold dependence on *Vtrim* for the sample of non-irradiated digital chips. The different colors represent different chips.

6 Summary

Within this thesis, irradiation effects on the analog *PSI46V2* and the digital *PSI46digV2* readout chip have been investigated. This included the study of irradiation effects on different calibration methods and on the *Vtrim* DAC. In addition a pulse height DAC optimization has been carried out for the digital chip before irradiation.

The calibration of irradiated chips revealed that the spectrum-method is prone to irradiation defects in the sensor which act as traps and cause a reduction of the charge collection efficiency. The obtained calibration slopes exceeded any reasonable outcome. Hence the dependence of the charge collection efficiency on irradiation has to be further studied in order to use the threshold method for calibration of irradiated chips.

To circumvent the influence of irradiation defects on the calibration, a new method has been developed based on the measurement of the band gap reference voltage. Irradiation induced shifts of this voltage are considered to be the main reason for changes of the *Vcal* calibration slope. An increase of the band gap reference voltage and hence of the calibration slope by about 10 % for the highest irradiation fluence was observed for analog chips, which is in agreement with previous studies. Additionally, these results were confirmed by the results from calibrating irradiated ROCs with non-irradiated sensors with X-rays.

The irradiation effects on *Vtrim* have been thoroughly investigated for the analog chip. After irradiation the ability of *Vtrim* to reduce the comparator threshold decreases. For very high irradiation fluence of $3 \times 10^{15}\,\mathrm{n}_{\mathrm{eq}}/\mathrm{cm}^2$ the threshold reduction yield of *Vtrim* is not sufficient anymore for a successful trimming. Based on the calibration results from irradiated ROCs with non-irradiated sensors, the changes of the *Vtrim* characteristics were further expressed in terms of electrons. In addition, the equivalent of one *Vtrim* DAC unit was determined in electrons for different irradiation levels.

The digital chips were analyzed before and after irradiation. Before irradiation the sample has been calibrated and pulse height DAC optimization has been carried out. A calibration slope of 51.04 ± 2.53 electrons per *Vcal* was obtained. *Vtrim* was expressed in electrons per DAC. During the first irradiation some of the chips have been powered. The following calibration, based on the band gap reference voltage method, revealed that powered chips were more affected by irradiation than unpowered ones, yielding a relative band gap reference voltage shift of 3.7 ± 2.2 %. For the unpowered chips a shift of 1.3 ± 2.3 % was observed. This observation is due to the behavior of irradiation defects in semiconductors in the presence of fields. Due to time constraints of this thesis the investigations of the digital sample were only realized for an irradiation fluence of $6 \times 10^{14}\,\mathrm{n}_{\mathrm{eq}}/\mathrm{cm}^2$ and should therefore be continued.

In conclusion, the new developed calibration method based on the band gap reference voltage measurements gives promising results for both analog and digital chips. Calibration of irradiated chips using the spectrum method has to be further studied. The *Vtrim* DAC characteristics after irradiation have been successfully investigated for the analog chips.

References

[1] S. Dambach. *CMS Pixel Module Readout Optimization and Study of the B^0 Lifetime in the Semileptonic Decay Mode.* PhD thesis, ETH Zurich, 2009.

[2] M. Dentan. Radiation effects on electronic components and circuits. *CERN Training: Radiation Effects on Electronic Components and Systems for the LHC*, 2000.

[3] C. Eggel. *CMS Pixel Module Qualification and Search for $B_s^0 \to \mu^+\mu^-$.* PhD thesis, ETH Zurich, 2009.

[4] D. Acosta et al. CMS Physics Techniqual Design Report Volume 1: Detector Performance and Software. Technical report, CMS Collaboration, 2006.

[5] G. Aad et al. Observation of a new Particle in the Search for the Standard Model Higgs Boson with the ATLAS Detector at the LHC. *Physics Letter B*, 716(1-29), 2012.

[6] L. Agostino et al. The CMS Experiment at the CERN LHC. *J. Instrum.*, 2008.

[7] P. Bryant et al. LHC Machine. *J. Instrum.*, 2008.

[8] S. Chatrchyan et al. Observation of a new Boson at a Mass of 125 GeV with the CMS Experiment at the LHC. *Physics Letter B*, 716(30-61), 2012.

[9] T. Rohe et al. Radiation Hardness of CMS Pixel Barrel Modules. *Nucl. Instr. and Methods in Physics Research Section A*, 624(2), 2010.

[10] J. Beringer et al. (Particle Data Group). Review of Particle Physics. *Physical Review D*, 86(1), 2012.

[11] P. Higgs. Broken Symmetries and the masses of Gauge Bosons. *Phys. Rev. Lett.*, (13):508–509, 1964.

[12] L. Hoppenau. Irradiation Effects on n-type and p-type Field Effect Transistors in a 0.25 μm Technology. Semester project, Paul Scherer Institut, 2012.

[13] H.-C. Kaestli. Private communication. Paul-Scherer-Insitut, July 2013.

[14] G. Lutz. *Semiconductor Radiation Detectors.* Springer, 1999.

[15] NIST, 07/20/2013. Xray transition energies. `http://www.nist.gov/pml/data/xraytrans/`.

[16] T. Rohe. Private communication. Paul-Scherer-Insitut, July 2013.

[17] L. Rossi, T. Rohe, D. Fischer, and N.Wermes. *Pixel Detectors.* Springer, 2006.

[18] LEP Working Group For Higgs Boson Searches. Search for the Standard Model Higgs at LEP. *Physics Letter B*, 565:61–75, 2003.

[19] The CMS Collaboration. Technical Proposal for the Upgrade of the CMS Detector trough 2020. Technical report, 2011.

[20] P. Trueb. *CMS Pixel Module Qualification and Monte-Carlo Study of $H \to \tau^+\tau^- \to l^+l^- E_T$.* PhD thesis, ETH Zurich, 2008.

[21] R. Wunsdorf. *Systematische Untersuchung zur Strahlenresistenz von Silizum-Detektoren für die Verwendung in Hochenerg-Experimenten.* PhD thesis, Hamburg University, 1992.

Appendix

Listing of the DACs on the *PSI46V2* and *PSI46digV2* readout chip which have been relevant in the context of this thesis [1]:

DAC	Type	Function
Vcal	8 bit	Provides an internal calibration signal, can be set to be to low or high range, high range being sevenfold larger than low range
CalDel	8 bit	Delays *Vcal*
Vana	8 bit	Regulates the analog current
Vdig	4 bit	Regulates the digital current on the chip
Vsf	8 bit	Regulates the low *Vcal* range linearity
VwllPr	8 bit	Regulates the feedback resistance of the preamplifier
VwllSh	8 bit	Regulates the feedback resistance of the shaper
VthrComp	8 bit	Sets the comparator threshold for all pixels
Vtrim	8 bit	Defines the range of the trim bits which are used to lower the global comparator threshold (set by *VthrComp*)
VhldDel	8 bit	Determines the sampling point of the sample and hold capacitance
IBias_DAC	8 bit	Stretches or squeezes the pulse height
VOffsetRO	8 bit	Shifts the pulse height vertically

Vcal calibration slope of analog ROCs using two or or three K_α lines [20]:

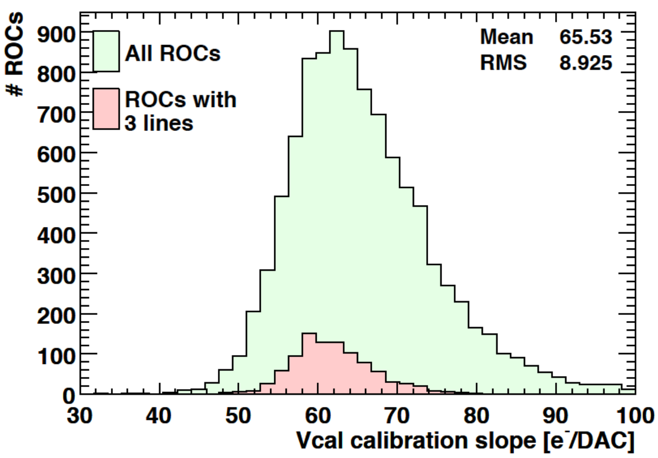

Measurements of the relative band gap reference voltage shift after gamma irradiation [12]. One MRad corresponds to about 3×10^{13} MIP/cm^2:

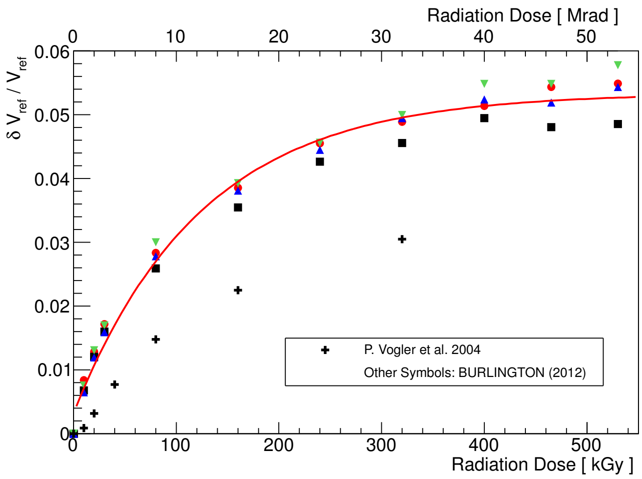

Measurements of the *Vdig* voltage with respect to the *Vdig* DAC for different irradiation fluences [9]: